DOI: 10.1002/ejic.200800644

Iron(III) Complexes of Metal-Binding Copolymers as Proficient Catalysts for Acid Hydrolysis of Phosphodiesters and Oxidative DNA Cleavage – Insight into the Rational Design of Functional Metallopolymers

Vasiliki Lykourinou,[a] Ahmed I. Hanafy,[a,b] Kirpal S. Bisht,[a] Alexander Angerhofer,[c] and Li-June Ming*[a]

Keywords: Heterogeneous catalysis / Hydrolysis / Iron / Metallopolymers / Phosphorus / DNA cleavage

Fe^{3+} complexes of pyridine-containing copolymers were found to be efficient and selective catalysts toward phosphodiester hydrolysis and show significant activity toward oxidative DNA cleavage. The catalysis toward bis(*p*-nitrophenyl)phosphate (BNPP) hydrolysis exhibits enzyme-like pre-equilibrium kinetics with maximum activities in the range of ca. pH 6–8 and a first-order catalytic proficiency (k_{cat}/k_o) of 4.2×10^7-fold at the acidic pH value of 5.3 (i.e., pK_a of the coordinated nucleophilic water) and 25 °C, entitling this Fe^{3+} copolymer an acid phosphodiester catalyst. This catalyst also shows significant selectivity toward BNPP hydrolysis relative to the hydrolyses of *p*-nitrophenyl phenylphosphonate and *p*-nitrophenylphosphate monoester, with a ratio of 4250:16:1 in terms of their first-order catalytic proficiencies at pH 8.0 and 25 °C. Fe^{3+} complexes of a few pyridine-containing copolymers show different hydrolytic activities, which points a direction for rational design of catalytic metallopolymers.

Introduction

Most linear copolymers are known for their inhomogeneous physical and chemical nature, such as the distribution of their chain lengths and random sequence. Nevertheless, bulk properties of copolymers can be quite well controlled and characterized, including their hydrophobicity/hydrophilicity, optical, magnetic, and electrochemical properties,[1] and physical shapes, which render wide applications of polymers. Despite their randomness, linear copolymers with specifically designed side chains can potentially serve the purpose for specific recognition as recently demonstrated, wherein some block copolymers exhibit high affinities toward specific target proteins with association constants in the order of 10^5–10^7 M^{-1}.[2] Here, the enzymatic "induced-fit" was suggested to play a role in the recognition. Such an enzyme-like phenomenon is suspected to also play a role in catalysis associated with polymer catalysts. Moreover, as polymers can be easily molded into different physical shapes such as films, nanoparticles, and porous particles, further applications can be envisioned. Several metal-binding polymers have recently been prepared and utilized as catalysts for different types of metal-centered reactions.[3] We have recently also demonstrated that a copolymer of vinylpyridine and acrylamide could bind metal ions and exhibit significant hydrolytic activities.[4] Therein, the pyridine group serves as the metal-binding ligand, and the amide group may provide specific recognition through hydrogen bonding. This copolymer thus may loosely mimic the active-site environment of various metalloenzymes.

Iron proteins[5] are best know to be involved in oxidation and/or oxygenation chemistry and to mediate electron transfer, such as ribonucleotide reductase, mono- and dioxygenases, peroxidases, and cytochromes. Numerous chemical models have been synthesized for the exploration of biological metal-centered chemistry on the basis that a mono- or dinuclear metal-binding site can be formed and a specific recognition site may possibly be built in. A number of Fe complexes of multidentate ligands have been prepared accordingly and exhibit various oxygenation and oxidation activities toward various organic compounds.[5,6] The action of some antibiotics capable of DNA binding and cleavage is also known to be dependent upon Fe,[7] such as anthracyclines and bleomycins. Conversely, fewer iron proteins are known to catalyze hydration and hydrolysis in biological systems. For example, nitrile hydratase[8] with a low-spin Fe^{3+} in the active site catalyzes the hydration of nitriles, whereas purple acid phosphatases[9] with a nonheme $Fe^{III}Fe^{II}$ or $Fe^{III}Zn^{II}$ active site catalyze nonspecific hydrolysis of phosphomonoesters. In metallohydrolases[10] and related synthetic model systems,[11] the high Lewis acidity of

[a] Department of Chemistry, University of South Florida, 4202 Fowler Avenue, CHE205, Tampa, Florida 33620-5250, USA
Fax: 813-974-1733
E-mail: ming@shell.cas.usf.edu
[b] Department of Chemistry, Faculty of science, Al-Azhar University, Nasr City, Cairo, Egypt
[c] Department of Chemistry, University of Florida, Gainesville, Florida 32611, USA

the metal center is responsible for a substantial decrease in the pK_a of the coordinated water and the generation of a nucleophile (in the form of hydroxide), which engenders hydrolytic activities of these systems around neutral pH or lower. Despite the very high Lewis acidity of Fe^{3+} and extensive investigation of Fe-centered oxidation and oxygenation chemistry, hydrolysis by Fe complexes has been much less explored.[12] We describe herein the exploration of Fe^{3+} complexes of pyridine-functionalized copolymers as versatile catalysts for phosphoester hydrolysis and oxidative DNA cleavage. A strategy for the design of metallopolymers for hydrolytic reactions is also discussed.

Results and Discussion

Metal Binding and Catalytic Stoichiometry

The pyridine- and acrylamide-containing copolymer family has been previously determined to bind various metal ions; however, detailed investigation of the coordination chemistry and catalytic properties was lacking.[13] We recently reported Cu^{2+} binding and hydrolytic activity of vinylpyridine–acrylamide copolymer **P1**.[4] This copolymer was also observed to readily bind Fe^{3+} in methanol to give a brown metallopolymer precipitate [which is quite distinct from the $Fe(OH)_3$ precipitate; see later]. Catalysis by this metallopolymer described herein is thus heterogeneous in nature. The activity of Fe^{3+}–**P1** toward the hydrolysis of 1.0 mM bis(*p*-nitrophenyl)phosphate (BNPP), a prototypical phosphodiester substrate, was determined as a function of various amounts of the complex in terms of the average repeating unit (RU) [Fe^{3+}-RU] under pseudo-first-order conditions in 1:1 methanol/buffer (25 mM HEPES) at pH 8.0 and 25 °C, from which a rate constant k_{obs} of $(2.92 \pm 0.08) \times 10^{-6}$ s^{-1} was obtained for the rate law rate = k_{obs}[Fe^{3+}-RU].

In order to determine the optimum metal-to-polymer stoichiometry for catalysis, a 1.0-mM RU aqueous methanol solution (50% methanol in 25 mM HEPES buffer at pH 8.0 and 25 °C) was titrated with freshly prepared methanol solution of Fe^{3+}, and the activity of the mixture was checked toward hydrolysis of 1.0-mM BNPP. A linear increase in activity upon the addition of Fe^{3+} was observed until one equivalent of Fe^{3+} was added with respect to [RU] (Figure 1), indicating that a 1:1 stoichiometry for metal binding to each RU is necessary for catalysis. Fitting of the activity with respect to the amount of the metal gives an apparent formation constant of 49000 M^{-1} for Fe^{3+}–**P1**.

To ensure that the observed activity is due to the insoluble metallopolymer complex, the heterogeneous Fe^{3+}–**P1**/methanol/buffer mixture was centrifuged and the solid and supernatant were evaluated for activity toward the hydrolysis of 1.0-mM BNPP. The activity of the supernatant was negligible, whereas the activity of the solid matched that observed for the initial heterogeneous mixture, confirming a heterogeneous catalysis. Although homogeneous catalysis is efficient and convenient in many cases, it suffers from difficulty in recovery of the catalyst and incorporation into a recycling or continuous flow process. These difficulties can be overcome by immobilizing catalytic centers on the surface of different matrices.[14] The iron–polymer system presented herein is one such example. Despite its extensive use in many types of reactions, heterogeneous catalysis has only scarcely been applied to hydrolytic processes[12d,4,15] and should be further explored.

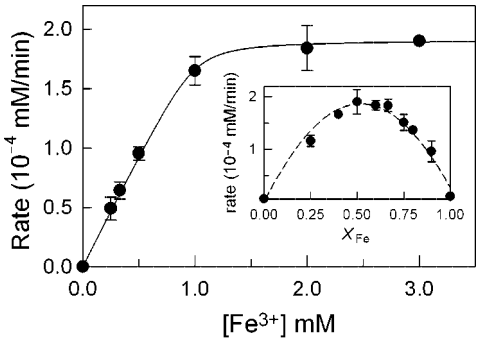

Figure 1. Titration of Fe^{3+} into 1.0 mM RU of copolymer $4Vp_3Ac_1$, monitored with the activity toward the hydrolysis of 1.0 mM BNPP in 50% methanol solution of 25 mM HEPES at pH 8.0 at 25 °C. Inset: Activity Job plot of Fe^{3+}–$4Vp_3Ac_1$ and numerical fitting to 1:1 complex, in which the initial rate of BNPP hydrolysis (1.0 mM) is plotted against X_{Fe} at a constant total concentration ([RU] + [Fe^{3+}]) of 2.0 mM and the activity monitored.

To further confirm the metal-to-polymer stoichiometry of the metallopolymer that exhibits the hydrolytic activity, a Job plot[16] was constructed. Because the Fe^{3+}–**P1** complex is not soluble, it cannot be monitored with optical absorption. Therefore, we modified the classic "optical Job plot" into an "activity Job plot", in which the activity toward the hydrolysis of BNPP instead of the optical density of the complex was determined with respect to the mol fraction of Fe^{3+} (X_{Fe}) or polymer RU ($X_{RU} = 1 - X_{Fe}$) at a constant total concentration [Fe^{3+}] + [RU] of 2.0 mM. The maximum in the activity Job plot is found at $X_{RU} \approx X_M \approx 0.5$ (Figure 1, inset), indicating that the predominant active species is an iron–polymer complex with a stoichiometry of Fe^{3+}/RU = 0.5:0.5 (1:1), which is consistent with the stoichiometry obtained from the titration of Fe^{3+} to the polymer (Figure 1).

Characterization with Electron Paramagnetic Resonance (EPR)

The X-band EPR spectrum of Fe^{3+}–**P1** shows the prototypical high-spin Fe^{3+} transition signals at $g = 4.26$ and $g = 2.07$, along with two broad signals at $g = 5.5$ and $g = 8$–9 and another two very broad signals in the high-field region at $g = 1.21$ and $g = 0.86$ (Figure 2). The $g = 4.26$ line indicates the presence of a completely rhombic (E/D, 1:3) high-spin Fe^{3+} ion, whereas the weaker features at higher and lower g values are often found in species with intermediate rhombic character ($E/D = 0.10$–0.20), in which three Kramers doublets give rise to the EPR spectrum. Typically, the linewidths of the signals at the highest fields are broadened the most, which is the case here. However, it should

be noted that excessive D-strain could also cause the appearance of a $g = 4.3$ line in an otherwise intermediately rhombic Fe^{3+}.[17] A value of D around 6000 MHz with a modest E ($E/D \approx 0.16$) shows weak lines at effective g values of 1.3 and 0.86 and stronger ones between g values of 5 and 12. The line at $g \approx 2$ can be most easily explained with a purely axial high-spin species, which would also give rise to significant spectral intensity at $g \approx 6$ for a large D of the order of 6000 MHz. Combined with a purely rhombic high-spin Fe^{3+} ion, which would explain the prominent line at $g \approx 4.3$, the major features of the spectrum can be qualitatively explained. A more definite determination of the g-factor and the fine-structure anisotropy will have to await a more detailed multifrequency study.

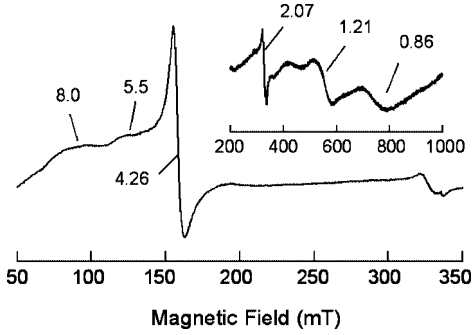

Figure 2. EPR spectrum of solid Fe^{3+}–**P1**. The inset shows the high-field features of the spectrum.

Kinetic Characterization of Phosphoester Hydrolyses

Although BNPP has been generally acknowledged to be quite accessible to hydrolysis due to the very good leaving group *p*-nitrophenol, its hydrolytic rate is still *extremely low* with a rate constant $k_o = 1.1 \times 10^{-11}$ s^{-1} at pH 7.0 and 25 °C,[18] that is, 1.1×10^{-10} s^{-1} at pH 8.0, considering OH^- as the nucleophile. Thus, the hydrolysis of BNPP by Fe^{3+}–**P1** shows a significant pseudo-first-order rate enhancement k_{obs}/k_o of 4.1×10^4 with respect to the noncatalyzed hydrolytic reaction of BNPP at pH 8.0.

In order to establish the rate law and catalytic proficiency for the heterogeneous hydrolysis of BNPP by Fe^{3+}–**P1**, the initial rates for the hydrolysis were determined in a range of 0.2–4.0 mM of the substrate at 25 °C and pH 8.0. The initial rate of BNPP hydrolysis can be determined from the linear increase in absorption at 405 mm with time (Figure 3A). To ensure efficient binding of the metal under all the experimental conditions during the kinetic studies (particularly at near-neutral and higher pH values, wherein Fe^{3+} can easily precipitate out of solution as hydroxides), an excess amount of the polymer was added into the reaction (RU/$Fe^{3+} \approx 2.5$ in terms of equivalents). The rate with respect to substrate concentration [S] is not linear (Figure 3B), which seems to follow the pre-equilibrium kinetics. The kinetics can be described as the binding of the substrate S to the metal center to form an intermediate S–Fe^{3+}–**P1** complex, followed by conversion of the bound substrate to the products [Equation (1)]. Owing to the heterogeneous nature of the catalysis, the pre-equilibrium stage is attributed to the binding of the substrate onto the surface of the Fe–**P1** complex. The reaction rate for this type of "surface reaction" is proportional to the surface area.[19] When the catalytic centers of the catalyst in a heterogeneous catalysis are well exposed, the rate is in turn proportional to the amount of the catalyst. The rate law for this pre-equilibrium surface reaction can be obtained with steady-state approximation and an assumption that the amount of the bound S is much less than that of the free S in solution, which is expressed [Equation (2)] analogously to enzyme catalysis, in which $K' = (k_{-1} + k_{cat})/k_1$ is the virtual dissociation constant of the bound S, equivalent to the Michaelis constant in enzyme catalysis. The data can be well fitted to Equation (2) to yield the rate constants $k_{cat} = (5.6 \pm 0.4) \times 10^{-6}$ s^{-1} (as the first-order rate constant at high [S] >> K') and $K' = 0.45 \pm 0.03$ mM, and a second-order rate constant (or the catalytic efficiency) $k_{cat}/K' = 0.0125$ M^{-1} s^{-1} at low [S] << K'. The good fit verifies the pre-equilibrium pathway for the catalysis shown in Equation (1), indicating direct substrate binding with the metallopolymer and a metal-centered hydrolytic catalysis. The results indicate that a catalytic proficiency[20,21] of 5.1×10^4 is obtained for the hydrolysis of BNPP at pH 8.0 in terms of first-order rate constants (k_{cat}/k_o), wherein $k_o = 1.1 \times 10^{-10}$ at pH 8.0 considering OH^- as the nucleophile,[18] and of an enormous 3.2×10^9 in terms of the catalytic efficiency $(k_{cat}/K_m)/k_w$,[22] wherein $k_w = k_o/27.8$ with 27.8 being the concentration of water in 50% aqueous methanol solution.

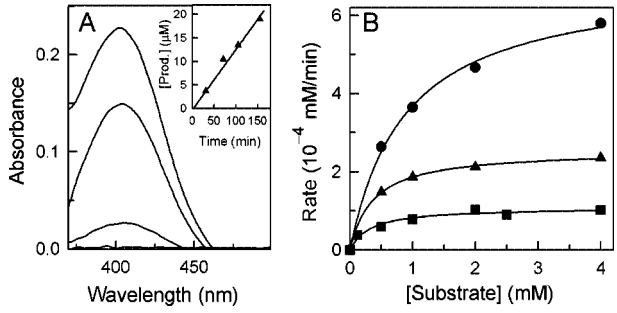

Figure 3. (A) A typical plot of the increase in absorption attributed to the hydrolysis of 1 mM BNPP by 0.4 mM [Fe^{3+}–RU] of the Fe^{3+}–$4Vp_3Ac_1$ complex at 75, 175, and 230 min after the metallopolymer is separated from the solution by centrifugation. The inset shows a linear plot for acquiring the initial rate (1 mM BNPP and 1 mM [Fe^{3+}–RU]). (B) Plot of the initial hydrolytic rates of NNP (■), BNPP (▲), and NPPP (●) by 0.8 mM [Fe^{3+}–RU] of the $4Vp_3Ac_1$ copolymer at pH 8.0 and 25 °C. The solid curves represent the best fit to the rate law of Equation (2).

$$Fe^{3+}\text{–}\mathbf{P1} + S \underset{k_{-1}}{\overset{k_1}{\rightleftharpoons}} S\text{–}Fe^{3+}\text{–}\mathbf{P1} \xrightarrow{k_{cat}} Fe^{3+}\text{–}\mathbf{P1} + Prod \quad (1)$$

$$rate = \frac{k_{cat}[Fe\text{–}RU][S]}{K' + [S]} \quad (2)$$

In addition to this phosphodiester substrate, Fe^{3+}–**P1** is also active toward the hydrolysis of the phosphomonoester

Table 1. Hydrolysis by Fe^{3+}–**P1**[a,g] and other Fe^{3+}–polymers[b–d] as well as Zn^{2+}–[e] and Cu^{2+}–**P1**.[f][4a]

Substrate	k_{cat} ($s^{-1} \times 10^{-6}$)	K' (mM)	k_{cat}/K' ($s^{-1}\,M^{-1}$)	CP[h]	Half life[h]
BNPP[a]	5.6 ± 0.4	0.45 ± 0.03	0.0125	5.1×10^4	1.4 d
BNPP[b]	0.15 ± 0.01	19.3 ± 0.1	7.88×10^{-6}	1380	52 d
BNPP[c]	4.30 ± 0.04	0.39 ± 0.05	0.011	3.9×10^4	1.9 d
BNPP[d]	7.90 ± 0.08	1.73 ± 0.10	4.56×10^{-3}	7.2×10^4	1.0 d
BNPP[e]	5.9 ± 0.4	0.70 ± 0.05	7.0×10^{-3}	4.5×10^4	1.4 d
BNPP[f]	8.30 ± 0.35	1.02 ± 0.15	8.3×10^{-3}	7.5×10^4	0.97 d
NPPP[a,g]	14.7 ± 1.8	0.95 ± 0.01	0.0154	193	13 h
NPP[a,g]	2.20 ± 0.11	0.30 ± 0.09	7.33×10^{-3}	27	3.6 d

[a] Hydrolysis of BNPP by Fe^{3+}–**P1**. Conditions: reaction volume = 2.5 mL in 25 mM HEPES at pH = 8.0 and 25 °C, [Fe^{3+}] = 0.8 mM, [polymer RU] = 3.2 mM. Substrates: [BNPP] = 0.3–6.0 mM, [NPP] = 0.13–2.5 mM, and [NPPP] = 0.5–10.0 mM. The substrates TNPP and Leu-*p*NA[23] are not hydrolyzed by Fe^{3+}–**P1**. [b] Hydrolysis by Fe^{3+}–**P1a** (i.e., desamido-**P1**) under the same conditions in [a]. [c] Hydrolysis by Fe^{3+}–**P9** (Py_5Ac_1) under the same conditions in [a]. [d] Hydrolysis by Fe^{3+}–$\mathbf{P_0}$ (poly-4-vinylpyridine) under the same conditions in [a]. [e] Hydrolysis by Zn–**P1** (this work). [f] Hydrolysis by Cu–**P1**. [g] Hydrolysis by Fe^{3+}–**P1**. [h] Catalytic proficiency (CP) is expressed in terms of the first-order rate constants (k_{cat}/k_o). The second-order CP can be obtained in terms of $(k_{cat}/K')/k_w$ described in the text. The autohydrolytic rate constant of BNPP k_o is 1.1×10^{-10} s^{-1} with a life time of 203 years, that of NPPP[24] is 7.65×10^{-8} s^{-1} with a life time of 3.5 months, and that of NPP[25] is 8.2×10^{-8} s^{-1} with a life time of 3.3 months.

p-nitrophenyl phosphate (NPP) and the phosphonate ester *p*-nitrophenylphenyl phosphonate (NPPP) (Figure 3 and Table 1), but not the phosphotriester tris(*p*-nitrophenyl) phosphate (TNPP) and a peptide mimic Leu-*p*-nitroanilide (Leu-*p*NA) under the same experimental conditions. The catalytic rate of hydrolysis follows the order NPPP > BNPP > NPP >> TNPP/Leu-*p*NA in terms of their rate constants k_{cat}. However, the autohydrolytic rate (k_o) of these phosphoesters follows the order Leu-*p*NA[23] ≈ NPP ≈ NPPP >> BNPP (Table 1), indicating a significant catalytic selectivity of Fe^{3+}–**P1** toward the phosphodiester BNPP with catalytic proficiency (k_{cat}/k_o) in the order of BNPP >> NPPP > NPP in a ration of 4250:16:1.

The pH is an important factor in hydrolytic reactions. The rate of hydrolysis increases with pH during base hydrolysis in aqueous solution, wherein the rate is proportional to the concentration of the nucleophile OH^-. To reveal the status of the nucleophile in Fe^{3+}–**P1**, the effect of pH on BNPP hydrolysis by Fe^{3+}–**P1** was investigated. This study is of interest, as Fe^{3+} ions form hydroxide coagulates in an aqueous environment even under acidic conditions, yet hydrolysis is in general more favorable at high pH values. Hydrolysis of 1.0 mM BNPP by Fe^{3+}–**P1** was studied in the pH range 4.5–10.0, affording a bell-shaped profile (Figure 4). Fitting of the data to the apparent two-ionization process [Equation (3)] reveals two ionization constants $pK_{a1} = 5.3 \pm 0.4$ and $pK_{a2} = 8.6 \pm 0.8$.

The first ionization can be assigned to the nucleophilic water molecule coordinated to the Fe^{3+} ion in the complex, because there is no other group that is expected to ionize around pH 5 to serve as a general base that can activate the hydrolytic catalysis. The pK_a values of phosphodiesters are near or less than 1 and the pK_a of the conjugated acid of pyridine is 5.2, which should significantly decrease upon metal binding. Thus, these two groups cannot contribute to pK_{a1} from the pH profile. The low pK_{a1} value can be attributed to the strong Lewis acidity of the Fe^{3+} center, like in the case of purple acid phosphatase.[9] The second deprotonation constant pK_{a2} is possibly associated with the formation of the iron hydroxide precipitate due to the small

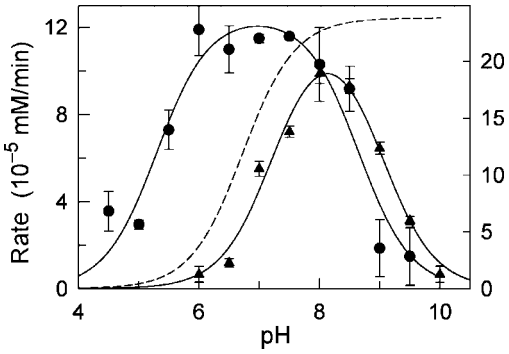

Figure 4. Effect of pH on the hydrolysis of 1.0 mM BNPP by 0.4 mM of Fe^{3+}–**P1** (●), 1.0 mM Zn^{2+}–**P1** (▲), and 1.0 mM Cu^{2+}–**P1** (dashed trace) in terms of metal concentration. The data are fitted to a two-ionization process according to Equation (3), in which only the first ionization produces the active form, V is the hydrolytic rate, V_{lim} is the rate for the deprotonated active species, and K_a's are the ionization constants.

$$V = V_{lim}/(1 + [H^+]/K_{a1})(1 + K_{a2}/[H^+]) \quad (3)$$

K_{sp} value (2.6×10^{-39}) of $Fe(OH)_3$ which was determined herein to be catalytically inactive under the experimental conditions. The K_{sp} value indicates that 1.0 mM Fe^{3+} would form $Fe(OH)_3$ precipitates at pH values as low as ≈2.1. The difference between the pH and pK_{a2} values reflects that Fe^{3+} is tightly bound to the polymer with an intrinsic affinity constant of $\approx 3.2 \times 10^6$ M^{-1} (i.e., $10^{-2.1}/10^{-8.6}$), which is 70 times higher than the binding affinity determined from metal-activity titration at pH 8.0 (Figure 1). Owing to the large magnitude, the latter measurement may not afford a more accurate value, as a small error at around 1 equiv. can cause a large deviation in the affinity constant. Thus, the pH profile provides a better estimate of the affinity constant for Fe^{3+} binding to **P1**.

The phospho-products generated in phosphoester hydrolysis are acidic. As a result, the pH of the reacting solution is expected to drop during the course of the reaction. Thus, a catalyst with a high activity in the acidic region is expected to be more efficient in phosphoester hydrolysis.

The low pK_a of 5.3 for BNPP hydrolysis by Fe^{3+}–**P1** renders this metallopolymer an ideal catalyst for phosphoester hydrolysis. For purpose of comparison, the pH profile of BNPP hydrolysis by Zn^{2+}–**P1** was acquired (▲, Figure 4). As for the pH profile of Fe^{3+}–**P1**, a bell-shaped pH profile was obtained with two pK_a values at 7.3 ± 0.1 and 9.0 ± 0.1, wherein the first is attributed to the nucleophilic water, whereas the second is likely to be attributed to the precipitation of $Zn(OH)_2$ as in the case of Fe^{3+}–**P1**. The pK_a for BNPP hydrolysis by Fe^{3+}–**P1** is two units lower than that of Zn^{2+}–**P1**, showing 50% activity at pH 5.3, whereas the latter is nearly inactive. Cu^{2+}–**P1** is also nearly inactive at pH 5.3 (pK_a = 6.7; dashed trace, Figure 4), despite the strong Lewis acidity of the Cu^{2+} center.[4a] These results further indicate the uniqueness of the Fe^{3+} center in acid hydrolysis of phosphoesters, as in the case of the enzyme purple acid phosphatase. Fe^{3+}–**P1** can thus serve as a functional model for an acid phosphatase.

The maximum rate of the catalysis V_{lim} in the pH profile is found in the range ca. pH 6.0–8.0 (Figure 4), which reflects that a catalytic proficiency[20,21] of the magnitude of 5×10^6 can be obtained for the hydrolysis of BNPP at pH 6.0 in terms of first-order rate constants (k_{cat}/k_o), wherein k_o is supposed to be 1.1×10^{-12} at pH 6.0 by considering OH^- as the nucleophile.[18] This result indicates that Fe^{3+}–**P1** is able to perform acid hydrolysis of phosphodiesters at pH < 6.0, which affords an enormous first-order catalytic proficiency of 4.2×10^7 at pH = 5.3 (i.e., the pK_a of the coordinated nucleophilic water in Fe^{3+}–**P1**). Herein, the rate can be estimated to be 2.32×10^{-6} mM/s, that is, one-half of V_{lim} from Figure 4, whereas k_o is estimated to be 2.2×10^{-13} as a result of the decrease in [OH^-] by a factor of five from pH 6.0 to pH 5.3. The catalytic proficiency at pH 5.3 and the rate constant at pH 8.0 are comparable or better than catalytic BNPP hydrolysis by several homogeneous and heterogeneous metal complexes and polymers under various conditions. For example, the mononuclear complexes $[(ethylenediamine)_2Co^{III}OH]^{2+}$ and [(1,4,7-triazacyclononane)$Cu^{II}OH]^+$ exhibit $k_{obs} = (3.0 \pm 1.0) \times 10^{-5}$ s^{-1} (50 °C) and $k_{obs} = (5 \pm 2) \times 10^{-7}$ s^{-1} (25 °C), respectively, at pH 7.2;[26] the dinuclear complexes $[Zn_2(BPAN)(\mu\text{-}OH)(\mu\text{-}O_2Ph_2)]^{2+}$ and $Cu_2(H_2bbppnol)(\mu\text{-}OAc)(H_2O)_2Cl_2$ exhibit $k_{cat} = (4.1 \pm 1.2) \times 10^{-6}$ s^{-1} and $k_{cat} = 5.4 \times 10^{-5}$ s^{-1} and K_m = 2 mM and K_m = 12 mM, respectively (pH 7.0 and 40 °C);[27] an acridine-containing di-Fe complex exhibits $k_{cat} = (5.2 \pm 0.2) \times 10^{-5}$ s^{-1} and $K_m = 3.1 \pm 0.1$ mM at pH 7.36 and 50 °C;[28] the metallopolymers Cu^{II}(vbpy)[29] and Cu^{II}(adenine) show $k_{cat} = 2.3 \times 10^{-5}$ s^{-1} (at 25 °C) and $k_{cat} = 2.23 \times 10^{-6}$ s^{-1} (at 30 °C) at pH 8.0;[30] Cu^{II}–**P1**[4] and Fe^{III}–Chelex resin[31] exhibit $k_{cat} = 8.30 \pm 0.35 \times 10^{-6}$ s^{-1} and $k_{cat} = 1.8 \times 10^{-7}$ s^{-1} at 25 °C and pH 8.0 and 9.0, respectively. Being able to perform acid hydrolysis of phosphoesters is catalytically significant, as the phosphate/phosphoesters products are acidic and can potentially slow down the reaction rate by lowering the pH.

The results obtained herein are consistent with a metal-centered mechanism for the hydrolysis of BNPP by this metallopolymer. However, whether the catalysis is mononuclear or multinuclear cannot be concluded from the results shown. However, the linear increase in activity with the addition of Fe^{3+} before reaching saturation (Figure 1) is not consistent with dinuclear catalysis that is expected to afford a sigmoidal trace in the metal binding-activity profile unless the system only forms dinuclear centers, as discussed in the study of metal binding to the dinuclear aminopeptidase from *Streptomyces griseus*.[32]

Catalyst Recycling

One advantage of heterogeneous catalysts is their easy separation and recycling. To demonstrate that the Fe^{3+}–**P1** catalyst is also reusable owing to its heterogeneous nature in reaction solution, the catalyst was recovered by centrifugation after a typical reaction toward the substrate BNPP at 1–4 mM, washed repeatedly with buffer and methanol, and then added to freshly prepared solutions of BNPP for activity determination. The recycled Fe^{3+}–**P1** complex was able to continuously catalyze the hydrolysis of BNPP, but it showed a small loss in its activity after recycling eight times, which however, can be attributed to ≈20% mass loss of the catalyst after the extensive recycling due to its powdery texture.

Molecular Mechanics Calculations

Molecular mechanics calculations were performed on a short piece of polymer of three RUs, which revealed that the metal is bound to the **P1** polymer through three pyridine units and three water molecules to adopt an octahedral geometry, preferably from adjacent RUs separated by 3–5 side chains to afford an energy around –200 kcal/mol for different binding modes (Figure 5). Binding of the metal

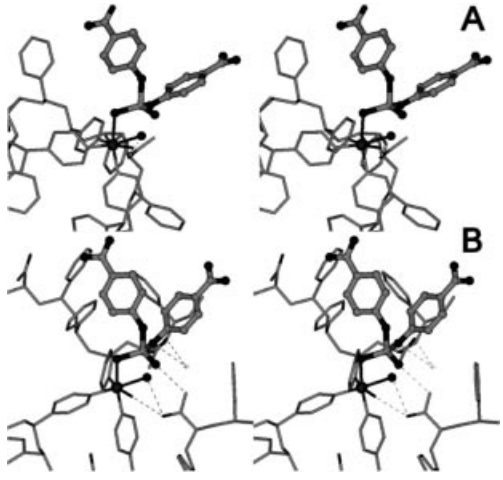

Figure 5. Molecular mechanics calculations of the metal-binding mode by using the MM3 protocol. The ligands are from each separated RU on the same polymer chain in panel A, whereas they are from different polymer chains in panel B. Herein, the metal adapts an octahedral geometry with three pyridine side chains, two water molecules, and a substrate. The nucleophilic water is represented with a solid sphere.

to pyridine units that are less than three side chains apart causes the coordination to significantly distort from an octahedral coordination and the coordinated pyridine ring to pucker. The third ligand can come from an adjacent RU (Figure 5A) or from a proximal polymer chain (Figure 5B) to show optimal coordination geometry. The formation of coagulates upon metal binding to the polymer suggests possibility that the polymer chains tangle together upon metal binding, likely resulting from interstand cross linkage through metal binding as in the latter binding mode (Figure 5B). The MM3 calculations on the cross-strand metal binding reveal that this binding mode is the most stable form with a total energy of –640 kcal/mol.

The saturation kinetics described above reflect that the substrate is bound to the active-site metal first before it is hydrolyzed. The binding of one oxygen of the phospho-center to the metal affords a configuration with the coordinated nucleophilic water (solid sphere) situated about 3.2 Å away from the phosphorus center at the *trans* position of the nitrophenol leaving group for an S_N2 pathway. Moreover, the amide group in this metallopolymer seems to serve as a general base to further activate the coordinated water and/or as a hydrogen-bond donor/acceptor to stabilize the bound substrate during the catalysis (particularly in the case of the interstrand metal binding; dashed lines, Figure 5B), thus further stabilizing the bound substrate to assist the hydrolytic activity.

Polymer Design

To provide more insight into the catalytic role of the auxiliary functional groups in copolymer **P1** toward hydrolytic activity, copolymers **P9**, **P1a**, and $\mathbf{P_0}$ were also used as ligands for the preparation of Fe^{3+}–polymer complexes and their hydrolytic activities checked. These copolymers contain functional groups other than amide, wherein **P9** has a slightly higher pyridine content (Py_5Ac_1) than **P1** on the basis of the NMR signals of the amide NH_2 protons,[4] **P1a** is the hydrolytic product of **P1** with the amide groups hydrolyzed to yield carboxylate groups, and $\mathbf{P_0}$ is poly-4-vinylpyridine. These copolymers can bind Fe^{3+} through the pyridine groups to form complexes that are expected to exhibit different hydrolytic activities from Fe^{3+}–**P1** owing to the difference in the nonmetal-binding auxiliary groups. Fe^{3+}–**P9** shows hydrolytic activity toward BNPP hydrolysis at pH 8.0 with $k_{cat} = (4.30 \pm 0.04) \times 10^{-6}$ s^{-1} and $K' = 0.39 \pm 0.05$ mM, comparable to Fe^{3+}–**P1**, whereas Fe^{3+}–$\mathbf{P_0}$ shows slightly higher k_{cat} and K' values at pH 8.0, $k_{cat} = (7.9 \pm 0.08) \times 10^{-6}$ s^{-1} and $K' = 1.73 \pm 0.10$ mM, respectively (Table 1). Although the k_{cat} value for the hydrolysis of BNPP by Fe^{3+}–**P1a** is 37 times lower than that by Fe^{3+}–**P1** at pH 8.0, K' is 43 times higher and the second-order rate constant k_{cat}/K' is more than 3 orders lower. Because $K' = (k_{cat}/k_1) + (k_{-1}/k_1)$, the significant decrease in k_{cat} and increase in K' in Fe–**P1a** relative to Fe–**P1** reflect a significant increase in (k_{-1}/k_1), the dissociation of the substrate–catalyst complex in Fe–**P1a**. This significant difference may be due to repulsion between the negatively charged BNPP and the carboxylate functional group in **P1a** at pH 8.0.

The amide group is suspected to be involved in H-bonding with the substrate through the NH_2 group, and probably with the coordinated water as a general base through the carbonyl group. If this H-bonding interaction is the sole difference between Fe^{3+}–**P1** and Fe^{3+}–**P1a** for stabilizing the transition state during the hydrolysis, the lack of H-bonding in the latter case would increase the activation energy by about 20 kJ/mol for an average H-bond energy, which would decrease the k_{cat} value by an approximate factor of 3000. The k_{cat} values for Fe^{3+}–**P1** and Fe^{3+}–**P1a** differ by only a factor of 37, indicating that there should be other interactions that are involved in transition-state stabilization and activity, such as the use of water molecules as "salt bridges" between the carboxylate group and the phosphoester substrate and/or the use of the carboxylate as a general base that interacts with the coordinated water and enhance the nucleophilicity of the water as found in many metallopeptidases.[33] Likewise, the uncoordinated pyridine side chains ($pK_a = 5.21$ for pyridine) in $\mathbf{P_0}$ may serve as a general base to enhance the nucleophilicity of the coordinated water molecules.

Inhibition of BNPP Hydrolysis by HPO_4^{2-}

Because the three different phosphoester bonds can be hydrolyzed by this complex with a small virtual dissociation constant K' for the bound substrate, it would be informative to evaluate the binding of a simple phosphate center to the complex. Phosphate is utilized here, which is the ultimate hydrolytic product of phosphoesters. Phosphate can significantly inhibit Fe^{3+}–**P1** toward the hydrolysis of 1.0 mM BNPP at pH 8.0 with an observed IC_{50} of ≈30 μM. The inhibition was further analyzed with the pre-equilibrium kinetics, which seems to exhibit a mixed inhibition pattern, but which is seemingly close to a noncompetitive pattern (Figure 6). The secondary plot from the Lineweaver–Burk plot yields the competitive inhibition constant $K_{ic} = 1.8 \pm 0.1$ μM and the uncompetitive inhibition constant $K_{iu} = 11.4 \pm 0.4$ μM for the dissociation of the inhibitor I from the complexes I–(Fe–**P1**) and I–(S–Fe–**P1**), respectively. Although these values obviously imply very effective inhibition, they are too low for the reaction catalyzed by 0.4 mM Fe–**P1** (lower than the stoichiometry). Thus, it is probable that part of the metal in the polymer is in its inactive form. Whether or not this is the case and, if so, how the amount of the active form of the catalyst can be enhanced await further exploration of different ways for the design and preparation of the catalyst.

The uncompetitive inhibition can also be attributed from deactivation of the catalyst as in the case of enzyme deactivation, such as binding of phosphate and removal of the metal from the polymer. To verify this hypothesis, the Fe^{3+}–**P1** complex was isolated by centrifugation after a typical reaction in the presence of 0.1 mM phosphate. The solid was washed with 1.0 M $CaCl_2$ to remove the phosphate, and then

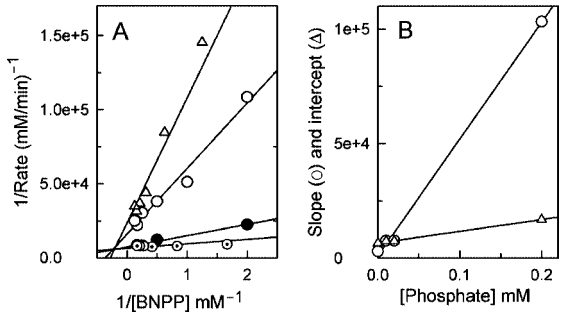

Figure 6. (A) Lineweaver–Burk plot of the inhibition toward BNPP hydrolysis by phosphate (at 0, 0.01, 0.02, and 0.20 mM from the bottom). (B) Secondary plots to reveal the inhibition constants K_{ic} (slope) and K_{iu} (intercept).

rinsed thoroughly. After addition of one equivalent of Fe^{3+} per RU, the activity was checked with saturating amounts of BNPP under typical reaction conditions and found to match the previously observed activity of the complex. This result confirms that phosphate inhibition can be partially due to removal of the metal from the active complex. Because the phospho-center (in the phosphoester substrates and phosphate) is demonstrated to interact with the Fe^{3+} complexes of copolymers **P1**, **P1a**, **P9**, and $\mathbf{P_0}$ (saturation kinetics and inhibition, respectively), it is interesting to investigate whether or not the phosphodiester bond in DNA can interact with this metallopolymer and whether or not cleavage can occur.

Oxidative Plasmid DNA Cleavage

DNA can undergo effective oxidative cleavage, and this can be monitored with agrose electrophoresis. An amount of 200-μM Fe^{3+} ions in 100 mM HEPES buffer at pH 8.0 and room temperature in the presence of 1.5%[34] (44 mM) H_2O_2 shows slow single-strand cleavage of the plasmid, yielding only nicked circular plasmid (top band in the top panel, Figure 7) within 120 min (lane 1′–6′). Herein, the cleavage by the simple Fe^{3+} ions is supposed to be random due to the lack of specific recognition rather than the basic electrostatic interactions, which thus serves as a reference for random DNA cleavage. The addition of a small amount of copolymer **P9** (38 μM) to the above reaction solution results in a significant enhancement in the oxidative cleavage of the plasmid. Therein, nicking of the supercoiled plasmid by Fe^{3+}–**P9** in the presence of 1.5% H_2O_2 occurs rapidly within 10 min (lane 1) with a trace amount of linearized form (3.5 kbp; center band), indicating efficient single-strand cleavage of DNA and possible double-strand cleavage. The linear form appears around 30 min (lane 3) and becomes much more obvious in the next 30 min (lane 4), which may result from extensive single-strand cleavage or may be attributed to the more relaxed/looser structure of the nicked circular form for easier access. Fe^{3+}–**P1** exhibits an oxidative nuclease activity (lanes 1 and 2 in bottom panel at 60 and 90 min, Figure 7) similar to that of Fe^{3+}–**P9**. Moreover, the presence of a small amount of a radical scavenger DMSO or mannitol (1.0 mM) slightly decreases the plasmid cleavage efficacy (lanes 3–6 at 60 and 90 min, bottom panel), suggesting possible generation of high-valent Fe center and free radicals in this oxidative plasmid cleavage. The use of the relatively low reagent concentrations in this case renders these Fe^{3+}–copolymer systems as efficient as Cu^{2+}–**P1** in DNA cleavage.[4a] Several $Fe^{2+/3+}$ complexes were previously reported to exhibit oxidative[35] and hydrolytic[28,36] activities toward DNA cleavage. The plasmid does not change for a period of 2 h in the absence of H_2O_2 in solution, reflecting that hydrolytic cleavage does not takes place to a noticeable extent under the experimental conditions and reagent concentrations.

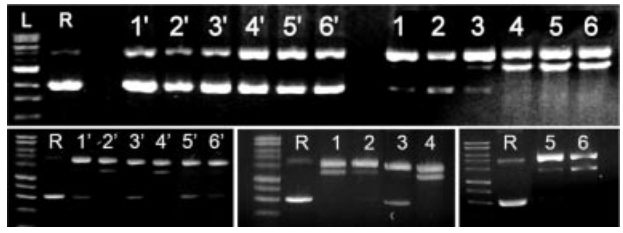

Figure 7. Top: Cleavage of plasmid DNA by Fe^{3+}–**P9** in the presence of 0.12 μg of plasmid DNA, 1.5% H_2O_2, and 210 μM of Fe^{3+} in 100 mM HEPES at pH 8.0 at time intervals of 10, 20, 30, 60, 90, and 120 min (lanes 1′–6′, respectively) and the above solutions in the presence of 38 μM **P9** RU under the same conditions (lanes 1–6, respectively). Lane R is the plasmid and lane L is the DNA reference with 0.5–5.0 kbp under the same conditions. The size of the linearized plasmid matches the marker of ≈3.5 kbp. Bottom: Influence of 1.0 mM DMSO (lanes 3, 4) and 1.0 mM mannitol (lanes 5, 6) on plasmid DNA cleavage by Fe^{3+}–**P1** (lanes 1, 2; 30 μM **P1** and 150 μM Fe^{3+} and 1.0% H_2O_2 in 50 mM HEPES buffer at pH 8.0) at 60 and 90 min, respectively, and by 150 μM Fe^{3+} (lanes 1′, 2′) and influence of 1.0 mM DMSO (lanes 3′,4′) and mannitol (lanes 5′,6′) at 60 and 90 min, respectively, under the same conditions as those used for Fe^{3+}–**P1**.

The activity toward double-stranded cleavage of plasmid may be attributed to the proximity of metal ions in the copolymer (which engenders a high local metal concentration) during the interaction of the polymer chain with the plasmid. Such a proximity effect in double-strand cleavage of DNA was also previously suggested to be the case in the cleavage of plasmid by Cu^{2+}–**P1**[4a] and a "bi-Fe^{2+}"[37] complex. In the latter case, two mononuclear Fe^{2+} complexes were connected by a linker 8–11 atoms in length to afford a dimer with two Fe^{2+} centers in close proximity.

Conclusions

We have shown that copolymers of vinylpyridine with different functional side groups can form complexes with Fe^{3+} that show activities toward phosphodiester hydrolysis to different extents, indicating that copolymers can be designed to form metallopolymers for different catalytic purposes. The effectiveness of Fe^{3+}–**P1** in phosphodiester hydrolysis is primarily due to the high Lewis acidity of the Fe^{3+} center, as demonstrated by the pH profile of the catalysis with a low pK_a of 5.3, which is presumably further aided by the amide functional group in the copolymer

chain. The amide group can be changed to different functional groups for possible finetuning of the catalytic properties, as demonstrated on the desamido form **P1a**. These metallopolymers are unique not only due to their catalytic efficiencies, which are comparable to homogeneous mononuclear and dinuclear complexes, but also due to their recycling capabilities and easy preparation, and these polymers are some of the very few examples of Fe-based systems for hydrolysis. Moreover, they are capable of activating hydrogen peroxide toward cleavage of plasmid DNA, which raises their potential use as "artificial chemical nucleases" and oxidative catalysts.

Experimental Section

Materials: The reagent 4-vinylpyridine was obtained from Acros Organics (Fair Lawn, NJ), acrylamide from BioRad (Richmond, CA), the buffers HEPES, CAPS, and MOPS, sodium acetate, Chelex, and the substrates BNPP, NPP, NPPP, TNPP, and Leu-*p*NA from Sigma–Aldrich (St Louis, MO). The buffer solutions were treated with Chelex resin to remove any trace amounts of metal ions.

Preparation and Identification of Copolymers and Fe^{3+} Complexes: The copolymer **P1** of 4-vinylpyridine (4Vp) and acrylamide (Ac) with an average repeating units (RU) of $4Vp_3Ac_1$ was prepared by the use of a 1:3 molar ratio of 4Vp/Ac in the presence of 1% molar amount of the initiator 2,2′-azoisobutyronitrile in DMF according to published procedures.[4] The formation of the copolymer was verified unambiguously by ^1H NMR spectroscopy (most acquired with a Bruker spectrometer at 250 MHz) to exhibit broad signals for the polymers and the disappearance of the sharp monomer signals. The stoichiometry of the RU can be determined on the basis of the integration of the ^1H NMR signals of the pyridine ring and the amide NH_2 protons.[4] The stoichiometry of $4Py_3Ac_1$ gives an apparent RU formula mass of 386.5 Da, which was used for the preparation of metal complexes and calculation of the mol fractions.

The use of a higher 4Vp/Ac ratio under the same conditions for the preparation of **P1** afforded a copolymer (**P9**) with stoichiometry of 4Vp/Ac, 5:1 ($4VP_5Ac_1$) for its RU based on ^1H NMR spectroscopy. The copolymer **P1a** of 4Vp and acrylic acid (Aa) with stoichiometry of $4Vp_3Aa_1$ for its RU was prepared directly from **P1** by base hydrolysis with 0.5 M NaOH solution, and verified by ^1H NMR spectroscopy to reveal the disappearance of the solvent exchangeable amide NH_2 signals. Poly-4-vinylpyridine was prepared as the other copolymers with 4-vinylpyridine.

Fe^{3+}–**P1** was prepared by addition of a slight excess amount of freshly prepared Fe^{3+} methanol solution into a methanol solution of **P1**. The metal-to-ligand stoichiometry was calculated on the basis of the polymer RU with the empirical formula of $4Py_3Ac_1$. The complex formed as a precipitate, which was washed with methanol to remove any loosely bound Fe^{3+}. Electron paramagnetic resonance (EPR) spectra of solid Fe^{3+}–**P1** were obtained with a Bruker Elexsys E580 cw/pulsed X-band spectrometer. For a typical cw EPR spectrum at ≈5–6 K, the field was set wide enough to reveal a possible low-field transition for magnetically coupled systems.

Computer Modeling: Molecular mechanics calculations of the metal-binding mode by using the MM3 protocol[38] were performed with the use of BioMedCAChe, version 6.1.10 (Fujitsu, Beaverton, Oregon). The coordination geometry of the metal was set to be octahedral, and the metal was considered to bind to pyridine in-plane with the pyridine ring. Any distortion from this coordination chemistry was considered to be an unfavorable metal-binding mode.

Kinetic Measurements: The initial rates of the hydrolysis of the substrates were monitored spectrophotometrically with a Varian Cary 50 or a Ultrospec1000 (Pharmacia Biotech) instrument within 2–5 h through the change at 405 nm due to the production of 4-nitrophenolate (17500 $M^{-1}cm^{-1}$). As the reaction is heterogeneous, the reaction mixture was centrifuged to separate the supernatant for optical measurement at certain time intervals. Various amounts of the complex and substrates were used in the reactions separately, from which rate laws were determined and rate constants obtained. Fe^{3+} ions (which readily precipitate out as rust under the experimental conditions herein) and copolymer solutions were used as the controls and showed negligible activity compared to Fe^{3+}–**P1**. The buffers utilized in the pH-activity profile were sodium acetate (pH 4.0–5.0), MES (pH 5.0–6.5) HEPES (pH 7.0–8.0), TAPS (8.5–9.0), and CAPS (pH 10.0) at 25 mM.

Oxidative Cleavage of Plasmid DNA: A volume of 10.0 μL of Fe^{3+}–**P1** (21.0 μM of Fe^{3+} and 3.8 μM **P1** RU in solution), 0.8 μL of 150 ng/μL plasmid DNA and 2.0 μL of 1% H_2O_2 (final concentration 0.15% or 44 mM) was incubated for several different time intervals. The reference samples contained the same concentrations of all the reagents but no polymer. All DNA (pQE30Xa plasmid; Quiagen) cleavage assays were buffered with 100 mM HEPES at pH 8.0. The experiment was repeated three times to ensure consistency. All plastic wares were demetallized with EDTA and washed several times with 18.2 MΩcm water. The oxidative cleavage of plasmid DNA was observed by using 1% agarose gel electrophoresis (150 V, 1 × Tris-Acetate buffer for 1 h), stained with ethydium bromide, and then photographed on a transilluminator.

Acknowledgments

A. I. H. acknowledges a fellowship and financial support from the Egyptian Government for conducting research overseas.

[1] a) M. Jaiswal, R. Menon, *Polym. Inter.* **2006**, *55*, 1371–1384; b) A. L. Stepanov, R. I. Khaibullin, *Rev. Adv. Mater. Sci.* **2004**, *7*, 108–125.
[2] S. J. Koch, C. Renner, X. Xie, T. Schrader, *Angew. Chem. Int. Ed.* **2006**, *45*, 6352–6355.
[3] J. Suh, *Acc. Chem. Res.* **2003**, *36*, 562–570.
[4] a) A. I. Hanafy, V. Lykourinou-Tibbs, K. S. Bisht, L.-J. Ming, *Inorg. Chim. Acta* **2005**, *358*, 1247–1252; b) V. Lykourinou, A. I. Hanafy, G. F. Z. da Silva, K. S. Bisht, R. W. Larsen, B. T. Livingston, A. Angerhofer, L.-J. Ming, *Eur. J. Inorg. Chem.* **2008**, 2584–2592.
[5] a) L. Que, R. Y. N. Ho, *Chem. Rev.* **1996**, *96*, 2607–2624; b) B. J. Wallar, J. D. Lipscomb, *Chem. Rev.* **1996**, *96*, 2625–2658; c) R. P. Hausinger, *Crit. Rev. Biochem. Mol. Biol.* **2004**, *39*, 21–68.
[6] a) L. Que, A. E. True, *Prog. Inorg. Chem.* **1990**, *38*, 97–200; b) M. Costas, M. P. Mehn, M. P. Jensen, L. Que, *Chem. Rev.* **2004**, *104*, 939–986; c) E. Y. Tshuva, S. J. Lippard, *Chem. Rev.* **2004**, *104*, 987–1012; d) C. Liu, M. Wang, T. Zhang, H. Sun, *Coord. Chem. Rev.* **2004**, *248*, 147–168.
[7] L.-J. Ming, *Med. Res. Rev.* **2003**, *23*, 697–762.
[8] T. Nagamune, J. Honda, W. D. Cho, N. Kamiya, Y. J. Teratani, *J. Mol. Biol.* **1991**, *220*, 221–222.
[9] a) N. Sträter, T. Klabunde, P. Tucker, H. Witzel, B. Krebs, *Science* **1995**, *268*, 1489–1492; b) L. W. Guddat, A. Mcalpine, D. Hume, S. Hamilton, J. DeJersey, J. L. Martin, *Struct. Fold Des.* **1999**, *7*, 757–767.

[10] W. N. Lipscomb, N. Sträter, *Chem. Rev.* **1996**, *96*, 2375–2433.
[11] a) E. Kimura, T. Koike, *Adv. Inorg. Chem.* **1997**, *44*, 229–261; b) E. Kimura, *Prog. Inorg. Chem.* **1994**, *41*, 443–491; c) E. L. Hegg, J. N. Burstyn, *Coord. Chem. Rev.* **1998**, *173*, 133–165.
[12] a) E. Willkinson, Y. Dong, L. Que Jr, *J. Am. Chem. Soc.* **1994**, *116*, 8394–8395; b) T. Tanase, C. Inoue, E. Ota, S. Yano, M. Takahashi, M. Takeda, *Inorg. Chim. Acta* **2000**, *297*, 18–26; c) A. Neves, H. Terenzi, R. Horner, A. Horn, B. Szpoganicz, J. Sugai, *Inorg. Chem. Commun.* **2001**, *4*, 388–391.
[13] K. E. Geckler, N. Arsalani, *J. Macromol. Sci. Pure Appl. Chem.* **1996**, *A33*, 1165–1179.
[14] J. M. Thomas, W. J. Thomas, *Principles and Practice of Heterogeneous Catalysis*, VCH, New York, **1997**.
[15] a) B. R. Bodsgard, J. N. Burstyn, *Chem. Commun.* **2001**, 647–648; b) S. G. Srivatsan, S. Verma, *Chem. Eur. J.* **2001**, *7*, 4–7; c) Q. Lu, A. Singh, J. R. Deschamps, E. L. Chang, *Inorg. Chim. Acta* **2000**, *309*, 82–90.
[16] D. C. Harris, *Qualitative Chemical Analysis*, 5th ed., Freeman, NY, **1997**.
[17] J. T. Weisser, *Inorg. Chem.* **2006**, *45*, 7736–7747.
[18] B. K. Takasaki, J. Chin, *J. Am. Chem. Soc.* **1995**, *117*, 8582–8585.
[19] F. Wilkinson, *Chemical Kinetics and Reaction Mechanisms*, Reinhold, New York, **1980**, ch. 8.
[20] A. Radzicka, R. Wolfenden, *Science* **1995**, *267*, 90–93.
[21] D. B. Northrop, *Adv. Enzymol. Relat. Areas. Mol. Biol.* **1999**, *73*, 25–55.
[22] P. J. O'Brien, D. Herschlag, *J. Am. Chem. Soc.* **1998**, *120*, 12369–12370.
[23] $k_o = 9.8 \times 10^{-8}$ s^{-1} in 0.1 M HEPES buffer at pH 8.0 and 30 °C. C. A. Altan, H. I. Park, L.-J. Ming, *Biochemistry* **2006**, *45*, 13779–13793.
[24] J. S. Loran, R. A. Naylor, A. Williams, *J. Chem. Soc. Perkin Trans. 2* **1977**, 418–420.
[25] D. H. Vance, W. Czarnik, *J. Am. Chem. Soc.* **1993**, *115*, 12165–12166.
[26] E. L. Hegg, S. H. Mortimore, C. Cheung, J. E. Huyett, D. R. Powel, J. N. Burstyn, *Inorg. Chem.* **1999**, *38*, 2961–2968.
[27] C. Liu, M. Wang, T. Zhang, H. Sun, *Coord. Chem. Rev.* **2004**, *248*, 147–168.
[28] X. Q. Chen, X. J. Peng, J. Y. Wang, Y. Wang, S. Wu, L. Z. Zhang, T. Wu, Y. K. Wu, *Eur. J. Inorg. Chem.* **2007**, 5400–5407.
[29] C. M. Hartshorn, A. Singh, E. L. Chang, *J. Mater. Chem.* **2002**, *12*, 602–605.
[30] S. G. Srivatsan, S. Verma, *Chem. Eur. J.* **2001**, *7*, 828–833.
[31] V. Lykourinou-Tibbs, A. Ercan, L. J. Ming, *Catal. Commun.* **2003**, *4*, 549–553.
[32] C. Hasselgren, H. I. Park, L.-J. Ming, *J. Biol. Inorg. Chem.* **2001**, *6*, 120–127.
[33] W. N. Lipscomb, N. Sträter, *Chem. Rev.* **1996**, *96*, 2375–2433.
[34] For comparison, over-the-counter H_2O_2 solution for household use in the U. S. is 3%.
[35] a) A. Mukherjee, S. Dhar, M. Nethaji, A. R. Chakravarty, *Dalton Trans.* **2005**, 349–353; b) F. Ben Allal El Amrani, L. Perelló, J. A. Real, M. González-Alvarez, G. Alzuet, J. Borrás, S. García-Granda, J. Montejo-Bernardo, *J. Inorg. Biochem.* **2006**, 1208–1218.
[36] a) X. Chen, J. Wang, S. Sun, J. Fan, S. Wu, J. Liu, S. Ma, L. Zhang, X. Peng, *Bioorg. Med. Chem. Lett.* **2008**, *18*, 109–113; b) A. Horn, I. Vencato, A. J. Bortoluzzi, R. Horner, R. A. N. Silva, B. Spoganicz, V. Drago, H. Terenzi, M. C. B. de Oliveira, R. Werner, W. Haase, A. Neves, *Inorg. Chim. Acta* **2005**, *358*, 339–351; c) C. Liu, S. Yu, D. Li, Z. Liao, X. Sun, H. Xu, *Inorg. Chem.* **2002**, *41*, 913–922; d) A. Neves, H. Terenzi, R. Horner, A. Horn, B. Szpoganicz, J. Sugai, *Inorg. Chem. Commun.* **2001**, *4*, 388–391; e) L. M. Schnaith, R. S. Hanson, L. Que, *Proc. Natl. Acad. Sci. U.S.A.* **1994**, *91*, 569–573.
[37] T. A. van den Berg, B. L. Feringa, G. Roelfes, *Chem. Commun.* **2007**, 180–182.
[38] N. L. Allinger, Y. H. Yuh, J. H. Lii, *J. Am. Chem. Soc.* **1989**, *111*, 8551–8566.

Received: June 26, 2008
Published Online: February 5, 2009

